J|A|C|S
ARTICLES

Published on Web 11/17/2009

Au Nanocrystal-Directed Growth of Au−Cu_2O Core−Shell Heterostructures with Precise Morphological Control

Chun-Hong Kuo,[†] Tzu-En Hua,[‡] and Michael H. Huang*,[†]

Department of Chemistry, National Tsing Hua University, Hsinchu 30013, Taiwan, and Institute of Physics, Academia Sinica, Nankang, Taipei 11529, Taiwan

Received August 3, 2009; E-mail: hyhuang@mx.nthu.edu.tw

Abstract: Formation of metal−semiconductor core−shell heterostructures with precise morphological control of both components remains challenging. Heterojunctions, rather than core−shell structures, were typically produced for metal−semiconductor composites. Furthermore, growth of semiconductor shells with systematic shape evolution using the same metal particle cores can also present a significant challenge. Here, we have synthesized Au−Cu_2O core−shell heterostructures using gold nanoplates, nanorods, octahedra, and highly faceted nanoparticles as the structure-directing cores for the overgrowth of Cu_2O shells by a facile aqueous solution approach. The gold nanoparticle cores guide the growth of Cu_2O shells with morphological and orientation control. Systematic shape evolution of the shells can be easily achieved by simply adjusting the volume of reductant added. For example, truncated cubic to octahedral Cu_2O shells were produced from octahedral gold nanocrystal cores. Unusual truncated stellated icosahedral and star column structures have also been synthesized. The heterostructures were found to be formed via an unusual hollow-shell-refilled growth mechanism not reported before. The approach has potential toward the preparation of other complex Cu_2O structures with well-defined facets.

Introduction

Fabrication of heterostructured nanoparticles with positional and morphological control of the components can be quite challenging. Pursuit of the formation of such heterostructures is driven not only by the synthetic challenges and aesthetic beauty of the products but also by the potential enhanced functions offered by the composite nanostructures. Binary metallic,[1−7] metal−metal oxide/chalcogenide,[8−15] and oxide/chalcogenide[16−19] systems have all been investigated. Among these reported systems, only bimetallic heterostructures with a good lattice match can form morphologically controlled core−shell nanoparticles, as in the case of the epitaxial overgrowth of cubic Pd shells on cubic Pt seeds.[1] Heterojunctions, rather than complete core−shell structures, were generally formed for metal−semiconductor and oxide/chalcogenide systems, primarily due to a large lattice mismatch. Thus, it remains a significant challenge to prepare metal-semiconductor core−shell nanostructures with well-defined shell morphologies. Furthermore, with the exception of the successful epitaxial growth of Au−Ag core−shell nanocrystals from octahedral, decahedral and plate-like Au seeds,[6] most studies have not investigated the rich structural variety of shells that may be produced by employing core particles of different shapes. Core−shell nanocrystals with unusual morphologies that are unattainable by other means can be synthesized. Another interesting aspect of this type of research that is far less explored is the morphological evolution of the shell structure from the same core particles. This may not be easily achieved, and addition of another reagent to the

[†] National Tsing Hua University.
[‡] Academia Sinica.

(1) Habas, S. E.; Lee, H.; Radmilovic, V.; Somorjai, G. A.; Yang, P. *Nat. Mater.* **2007**, *6*, 692–697.
(2) Fan, F.-R.; Liu, D. Y.; Wu, Y.-F.; Duan, S.; Xie, Z.-X.; Jiang, Z.-Y.; Tian, Z.-Q. *J. Am. Chem. Soc.* **2008**, *130*, 6949–6951.
(3) Lim, B.; Wang, J.; Camargo, P. H. C.; Jiang, M.; Kim, M. J.; Xia, Y. *Nano Lett.* **2008**, *8*, 2535–2540.
(4) Xue, C.; Millstone, J. E.; Li, S.; Mirkin, C. A. *Angew. Chem., Int. Ed.* **2007**, *46*, 8436–8439.
(5) Xiang, Y.; Wu, X.; Liu, D.; Jiang, X.; Chu, W.; Li, Z.; Ma, Y.; Zhou, W.; Xie, S. *Nano Lett.* **2006**, *6*, 2290–2294.
(6) Tsuji, M.; Matsuo, R.; Jiang, P.; Miyamae, N.; Uemaya, D.; Nishio, M.; Hikino, S.; Kumagae, H.; Kamarudin, K. S. N.; Tang, X.-L. *Cryst. Growth Des.* **2008**, *8*, 2528–2536.
(7) Pellegrino, T.; Fiore, A.; Carlino, E.; Giannini, C.; Cozzoli, P. D.; Ciccarella, G.; Respaud, M.; Palmirotta, L.; Cingolani, R.; Manna, L. *J. Am. Chem. Soc.* **2006**, *128*, 6690–6698.
(8) Mokari, T.; Rothenberg, E.; Popov, I.; Costi, R.; Banin, U. *Science* **2004**, *304*, 1787–1790.
(9) Sun, Z.; Yang, Z.; Zhou, J.; Yeung, M. H.; Ni, W.; Wu, H.; Wang, J. *Angew. Chem., Int. Ed.* **2009**, *48*, 2881–2885.
(10) Shi, W.; Zeng, H.; Sahoo, Y.; Ohulchanskyy, T. Y.; Ding, Y.; Wang, Z. L.; Swihart, M.; Prasad, P. N. *Nano Lett.* **2006**, *6*, 875–881.
(11) Mokari, T.; Sztrum, C. G.; Salant, A.; Rabani, E.; Banin, U. *Nat. Mater.* **2005**, *4*, 855–863.
(12) Yang, J.; Elim, H. I.; Zhang, Q.; Lee, J. Y.; Ji, W. *J. Am. Chem. Soc.* **2006**, *128*, 11921–11926.
(13) Gu, H.; Zheng, R.; Zhang, X.; Xu, B. *J. Am. Chem. Soc.* **2004**, *126*, 5664–5665.
(14) Yu, H.; Chen, M.; Rice, P. M.; Wang, S. X.; White, R. L.; Sun, S. *Nano Lett.* **2005**, *5*, 379–382.
(15) Habas, S. E.; Yang, P.; Mokari, T. *J. Am. Chem. Soc.* **2008**, *130*, 3294–3295.
(16) Kwon, K.-W.; Shim, M. *J. Am. Chem. Soc.* **2005**, *127*, 10269–10275.
(17) Buonsanti, R.; Grillo, V.; Carlino, E.; Giannini, C.; Curri, M. L.; Innocenti, C.; Sangregorio, C.; Achterhold, K.; Parak, F. G.; Agostiano, A.; Cozzoli, P. D. *J. Am. Chem. Soc.* **2006**, *128*, 16953–16970.
(18) Kudera, S.; Carbone, L.; Casula, M. F.; Cingolani, R.; Falqui, A.; Snoeck, E.; Parak, W. J.; Manna, L. *Nano Lett.* **2005**, *5*, 445–449.
(19) Teranishi, T.; Inoue, Y.; Nakaya, M.; Oumi, Y.; Sano, T. *J. Am. Chem. Soc.* **2004**, *126*, 9914–9915.

Scheme 1. Schematic Illustration of Synthesis of Au−Cu_2O Core−Shell Heterostructures[a]

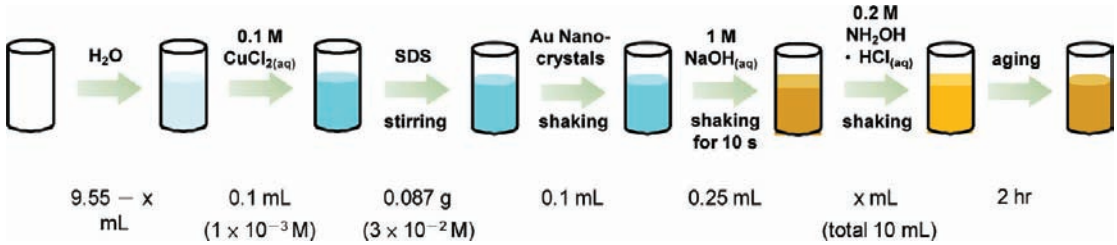

[a] Here x equals 0.15, 0.25, 0.45, and 0.65. The final concentrations of $CuCl_2$ and SDS are also given. The colors shown are the approximate solution colors observed.

pregrown core−shell polyhedra may be necessary to alter their final shapes.[1]

We have previously synthesized Cu_2O nanocrystals with systematic shape evolution from cubic to octahedral structures by a facile aqueous solution approach.[20] The successful preparation of these nanocrystals with well-defined shapes allows for examination of their facet-specific photocatalytic activity.[20–22] Interestingly, novel Cu_2O nanocages and nanoframes can be fabricated by using the same synthetic procedure but with the addition of HCl.[23] Octahedral Au nanocrystals and nanorods have been encapsulated within the nanocages. The ability of Cu_2O nanocrystals to accommodate single gold nanostructures suggests the possibility of fabricating a variety of Au−Cu_2O core−shell structures with good structural integrity. Here we report the syntheses of novel Au−Cu_2O core−shell nanostructures using Au nanoplates, nanorods, octahedra, and highly faceted nanoparticles as the structure-directing cores for the overgrowth of Cu_2O crystals. These gold nanostructures were prepared by following or adapting our reported procedures.[24−27] In all cases, the gold nanoparticles were found to be in the center of the final heterostructures. Some complex but highly symmetrical shell morphologies were generated. Remarkably, by simply varying the volume of $NH_2OH\cdot HCl$ reductant added, systematic shape evolution of the products can be easily achieved. This level of exquisite morphological control of metal−semiconductor core−shell structures and the ability for a wide range of structural variation are unprecedented. Furthermore, our examination of the growth process of the heterostructures revealed a surprising hollow-shell-refilled mechanism never reported before.

Experimental Section

Methods used for the preparation of Au nanoplates, nanorods, octahedra, and highly faceted Au nanoparticles are summarized in Supporting Information. All Au nanocores were finally dispersed in 0.5 mL of deionized water. In a typical synthesis of Au−Cu_2O core−shell heterostructures, $9.55 - x$ mL of deionized water, 0.1 mL of 1×10^{-3} M $CuCl_2$ solution, 0.087 g of sodium dodecyl sulfate (SDS), 0.1 mL of the Au nanocore solution, and 0.25 mL of 1 M NaOH were introduced into a sample vial in the order listed. Here x is the volume of $NH_2OH\cdot HCl$ added, and it can vary from 0.15 to 0.65 to obtain different shell morphologies. The total solution volume is 10 mL. After addition of a particular volume of 0.2 M $NH_2OH\cdot HCl$, the solution color became yellow and finally light brown when the mixture was aged for 2 h. To collect the products, all solutions were washed with deionized water and centrifuged four times at 3000 rpm for 5 min to remove the surfactant. The precipitate was dispersed in 0.5 mL of ethanol. For the observation of the intermediate products formed, 1 μL of the reaction mixture was withdrawn and transferred to a copper grid.

The structure and composition of the samples were studied by X-ray diffraction (XRD; Cu Kα radiation, Shimadzu XRD-6000), scanning electron microscopy (SEM; JEOL JSM-7000F), transmission electron microscopy (TEM; JEOL JEM-2100), high-resolution transmission electron microscopy (HR-TEM; JEOL JEM-3000F), high-angle annular dark-field scanning transmission electron microscopy (HAADF-STEM; JEOL JEM-2100), and energy-dispersive X-ray spectroscopy (EDS) techniques. UV−vis absorption spectra were taken on a Jasco V-570 spectrophotometer. A Leica Ultracut EM UC6 ultramicrotome was used for making cross-section samples.

Results and Discussion

The Au−Cu_2O core−shell heterostructures were synthesized by simply preparing a mixture of $CuCl_2$, sodium dodecyl sulfate (SDS) surfactant, Au nanocrystals, NaOH, and $NH_2OH\cdot HCl$ aqueous solution, added in the order listed, and aging the mixture for 2 h. The synthetic procedure is illustrated in Scheme 1. The copper ions should all turned into $Cu(OH)_2$ colloidal particles before being reduced to form Cu_2O. If the reaction time is not sufficiently long (that is, less than 2 h), some $Cu(OH)_2$ particles may still be in the solution.[22] SEM images of the Au nanoplates, nanorods, octahedra, and highly faceted nanoparticles serving as the structure-directing cores can be found in Supporting Information, Figure S1. Figure 1 shows the SEM and TEM images of the Au−Cu_2O core−shell nanocrystals. Uniform shell growth has been achieved for the samples. Every composite nanocrystal contains just one Au nanoparticle inside. With the introduction of 0.25 mL of 0.2 M $NH_2OH\cdot HCl$ solution, octahedral gold nanocrystals with sizes of 80 to over 100 nm developed into cuboctahedral Au−Cu_2O heterostructures (Figure 1a,b). A detailed TEM analysis on a single cuboctahedral nanocrystal indicates that the shell is composed of crystalline Cu_2O (see Supporting Information, Figure S2). The octahedral gold core has an orientation with its six corners aligned perpendicular to the six {100} faces of the cuboctahedral Cu_2O shell, strongly suggesting that the shell growth is precisely guided by the shape of the metal core. The highly faceted gold nanocrystals synthesized here with sizes of around 100 nm have somewhat different appearances and less distinct shapes. They are not necessarily centrally symmetric and are slightly elongated

(20) Kuo, C.-H.; Huang, M. H. *J. Phys. Chem. C* **2008**, *112*, 18355–18360.
(21) Kuo, C.-H.; Chen, C.-H.; Huang, M. H. *Adv. Funct. Mater.* **2007**, *17*, 3773–3780.
(22) Ho, J.-Y.; Huang, M. H. *J. Phys. Chem. C* **2009**, *113*, 14159–14164.
(23) Kuo, C.-H.; Huang, M. H. *J. Am. Chem. Soc.* **2008**, *130*, 12815–12820.
(24) Chu, H.-C.; Kuo, C.-H.; Huang, M. H. *Inorg. Chem.* **2006**, *45*, 808–813.
(25) (a) Wu, H.-Y.; Huang, W.-L.; Huang, M. H. *Cryst. Growth Des.* **2007**, *7*, 831–835. (b) Wu, H.-Y.; Chu, H.-C.; Kuo, T.-J.; Kuo, C.-L.; Huang, M. H. *Chem. Mater.* **2005**, *17*, 6447–6451.
(26) Chang, C.-C.; Wu, H.-L.; Kuo, C.-H.; Huang, M. H. *Chem. Mater.* **2008**, *20*, 7570–7574.
(27) Kuo, C.-H.; Chiang, T.-F.; Chen, L.-J.; Huang, M. H. *Langmuir* **2004**, *20*, 7820–7824.

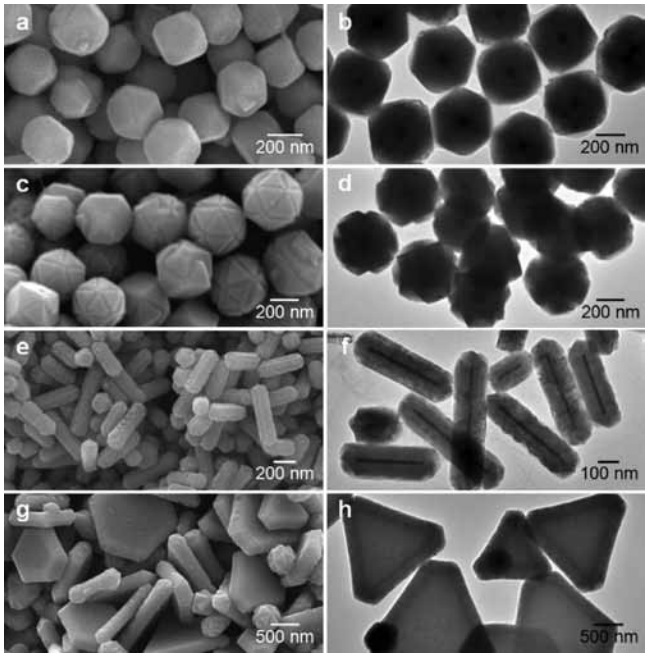

Figure 1. SEM and TEM images of Au−Cu_2O core−shell nanocrystals. (a, b) Cuboctahedral heterostructures made from octahedral Au nanoparticle cores. (c, d) Truncated stellated icosahedra formed from highly faceted Au nanoparticle cores. The slight structural variation observed may be related to the morphological variety of the gold nanoparticles used. (e, f) Cu_2O shells with pentagonal prism shape from 5-fold-twinned Au nanorods as templates. Barlike protrusions can be seen along the side faces of the pentagonal prism heterostructure. (g, h) Thick truncated triangular Cu_2O plates formed from triangular and truncated triangular Au plates as templates. The Cu_2O plates are slightly concave with thinner central triangular portions.

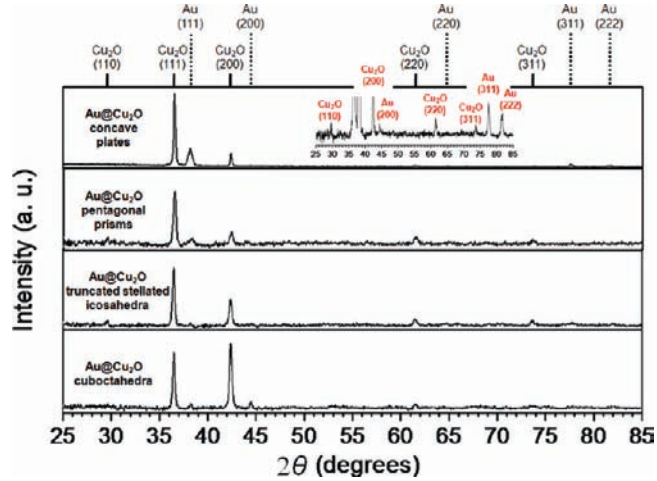

Figure 2. XRD patterns of different Au−Cu_2O core−shell heterostructures. Reflection peaks are generally weak for the Au cores except for the concave plates. (Inset) Expanded XRD pattern for the concave plates to clearly show the intensities of the Au peaks. The high intensity of the Cu_2O (200) peak for the Au−Cu_2O cuboctahedra is ascribed to their significant {100} faces.[20]

with twin defects. Unusual truncated stellated icosahedra were produced from these highly faceted gold nanocrystals as the metal cores (Figure 1c,d). Each structure contains 20 protruded triangular faces. This feature distinguishes them from the more typical icosahedral structure with flat faces. When gold nanorods with high aspect ratios were employed as the metal cores, elongated shells completely enclosing the rods were formed (Figure 1e,f). The gold nanorods have a pentatwinned structure, and the thick Cu_2O shells also develop into a similar pentagonal prism shape with five side protrusions running along the length of the heterostructures. This is another unusual nanostructure morphology not seen before. Finally, by use of micrometer- and submicrometer-sized triangular, truncated triangular, and hexagonal gold plates as the templating cores, conformal growth of Cu_2O shells was observed (Figure 1g,h). The edges of the Cu_2O shells are slightly thicker than the central portions, so the heterostructures are slightly concave. A few stellated icosahedra were also found, presumably because polyhedral gold particles were also synthesized in the preparation of the Au plates. TEM analysis of individual heterostructures formed from gold nanorods and plates as the metal cores also revealed the crystalline nature of the Cu_2O shells (see Supporting Information, Figure S2). It should be noted that only sufficiently large gold nanocrystals (preferably a few tens of nanometers) can be used to produce this precise shape-directing effect.

Further structural characterization of the Au−Cu_2O core−shell heterostructures was performed by XRD and EDS techniques. The XRD patterns of these heterostructures show strong Cu_2O reflection peaks and weak Au reflection peaks resulting from the core−shell nature of the particles (see Figure 2). Au−Cu_2O concave plates have thinner shells in the central portions, so intensity of the Au (111) reflection peak is relatively strong. EDS line scans of the various Au−Cu_2O core−shell heterostructures reveal strong Cu and O signals across the entire particles (see Supporting Information, Figure S3). The signals for Au appear only in the central regions of the particles where the gold cores are located. HAADF-STEM was also used to examine the core−shell particles with enhanced image contrast (see Supporting Information, Figure S4). The corresponding EDS elemental mapping images were taken. The EDS mapping images of the four kinds of Au−Cu_2O heterostructures again show that the elemental distribution matches with the HAADF-STEM images obtained.

To investigate the epitaxial growth interfaces of the core−shell heterostructures, the particles were sectioned by an ultramicrotome to reveal their cross-sectional views. Figure 3 gives the cross-sectional TEM images and the interfacial HR-TEM images of the four heterostructures synthesized. Again the gold nanocrystals were found to be located at the centers of the composite nanostructures. The orientation relationship between the core and the shell can be clearly identified for the cases with octahedral nanocrystals and pentatwinned nanorods as the structure-directing cores. The (111) planes of Cu_2O were found to grow epitaxially on the {111} facets of gold for most of the cases examined, while the (200) planes of Cu_2O can grow over the {200} facets of gold to form the interfaces. Interestingly, the lattice mismatch between the (111) planes of Au and the (111) planes of Cu_2O is about 4.5%, and 4.7% between the (200) planes of Au and the (200) planes of Cu_2O. Furthermore, the (111) planes of Cu_2O contain only copper atoms with a Cu−Cu distance of 3.01 Å, while the Au−Au distance on the (111) planes of gold is 2.88 Å as determined by use of the Diamond 3.0 program.[22] Here the interfacial lattice mismatch is about 4.3%. These lattice mismatch percentages are considered rather large for epitaxial growth of core−shell structures.[1] However, conformal epitaxial growth of Au@Pt nanocrystals with a large lattice mismatch of 4.71% has been achieved.[2] The analysis suggests that despite the presence of a significant mismatch between Au and Cu_2O lattice planes, Au−Cu_2O core−shell

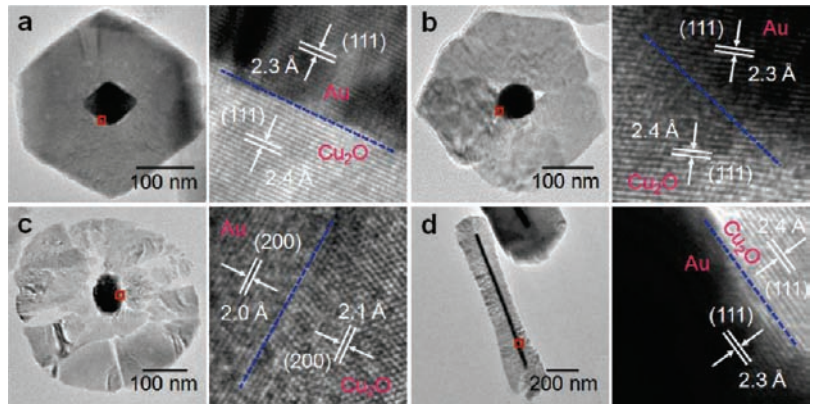

Figure 3. Cross-sectional TEM and interfacial HR-TEM images (red square regions) of the Au−Cu_2O core−shell heterostructures from (a) octahedral Au nanocrystals, (b) Au nanorods, (c) highly faceted Au nanoparticles, and (d) Au plates as templating cores. The (111) planes of Cu_2O were found to grow epitaxially on the {111} facets of gold, while the (200) planes of Cu_2O can grow over the {200} facets of gold to form the interfaces. The truncated stellated icosahedron may be more prone to fracture when subjected to the microtomy procedure, as seen in panel c.

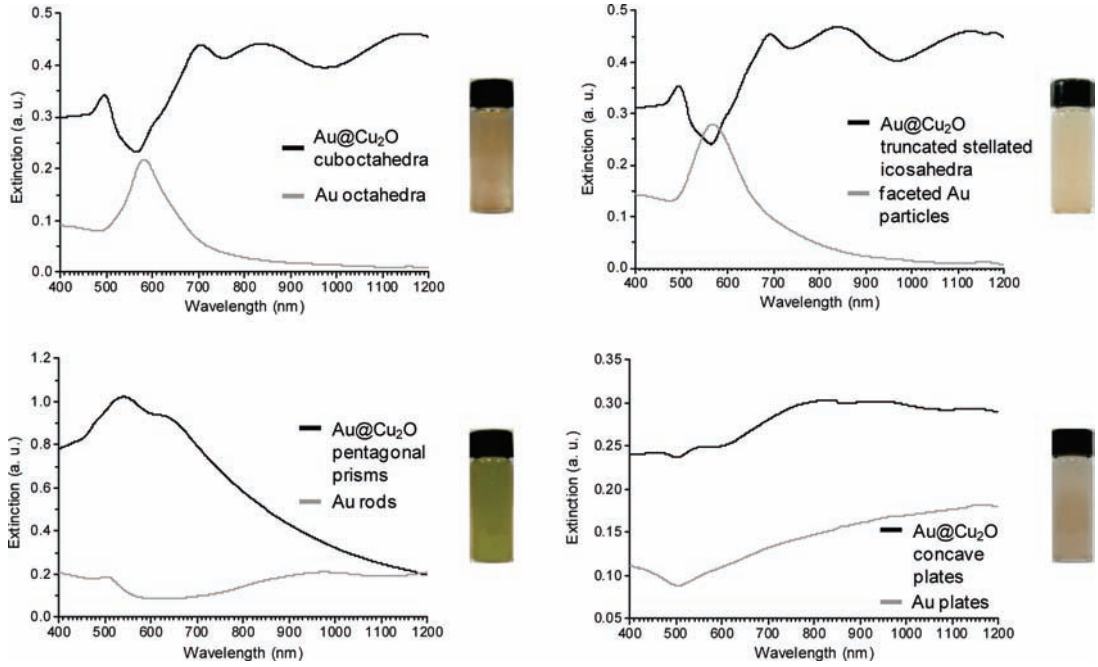

Figure 4. UV−vis spectra of various Au nanostructures and Au−Cu_2O core−shell structures. After formation of Au−Cu_2O hybrid structures, the unique SPR absorption of the Au nanostructures disappears. The spectral feature largely reflects only the absorption characteristics of Cu_2O crystals with a weak band gap absorption band at ∼500 nm and broad light scattering bands in the red and near-infrared regions due to the large particle sizes. The solution color for the core−shell pentagonal prisms is yellowish-green, while all other samples show an orange hue. This may be due to the special morphology of the rods making the incident light scattering at shorter wavelengths.

heterostructures with excellent interfacial epitaxial growth can still be prepared.[28]

Optical properties of the Au−Cu_2O heterostructures have been studied by taking the UV−vis absorption spectra of various gold nanocrystal cores and the heterostructures formed from these gold particles (see Figure 4). Remarkably, surface plasmon resonance (SPR) absorption bands of the gold nanocrystals disappeared. Only the characteristic absorption feature of Cu_2O crystals with a weak band gap absorption band at ∼500 nm and broad light scattering bands in the red and near-infrared regions due to the large particle sizes were recorded for the core−shell heterostructures. The spectral results provide strong evidence that essentially all the gold nanocrystals have turned into core−shell particles.

Previously we have demonstrated the systematic shape evolution of Cu_2O crystals from cubic to octahedral structures by simply varying the amount of $NH_2OH{\cdot}HCl$ used in the reaction mixture.[20,22] We discovered that the same procedure can also be applied to make Au−Cu_2O core−shell structures with systematic morphological evolution. Figure 5 shows the SEM images of the heterostructures synthesized by varying the volume of 0.2 M $NH_2OH{\cdot}HCl$ used from 0.15 to 0.25, 0.45, and 0.65 mL. Truncated cubes, cuboctahedra, truncated octahedra, and octahedra were synthesized from octahedral gold nanocrystal cores. The same shape evolution of Cu_2O crystals was also observed without the addition of the octahedral gold nanocrystals.[20] Unusual stellated icosahedra were prepared by use of highly faceted particle cores and the addition of 0.15 mL of 0.2 M $NH_2OH{\cdot}HCl$. Each of the 20 triangular faces of the particle develops into a triangular pyramid. This complex

(28) Wang, Y. Q.; Nikitin, K.; McComb, D. W. *Chem. Phys. Lett.* **2008**, *456*, 202–205.

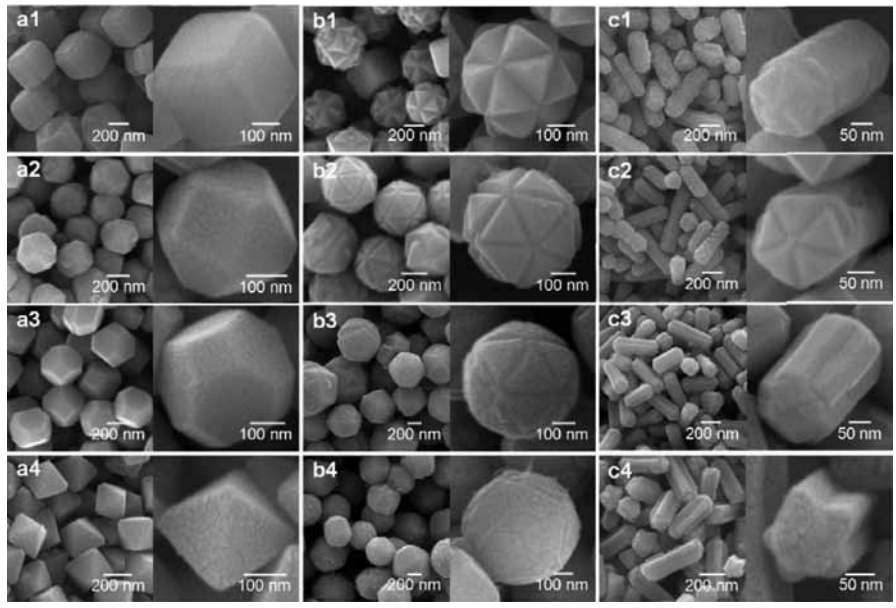

Figure 5. SEM images showing the systematic morphological evolution of Au−Cu_2O core−shell heterostructures. By gradually increasing the volume of 0.2 M $NH_2OH \cdot HCl$ used in the synthesis of Au−Cu_2O core−shell heterostructures from 0.15 to 0.25, 0.45, and 0.65 mL, (a1) truncated cubes, (a2) cuboctahedra, (a3) truncated octahedra, and (a4) octahedra were synthesized from octahedral Au nanocrystal cores. (b1) Stellated icosahedra were prepared by use of highly faceted particle cores and the addition of 0.15 mL of 0.2 M $NH_2OH \cdot HCl$. (b2) Truncated stellated icosahedra were produced by adding 0.25 mL of $NH_2OH \cdot HCl$. For further suppression of the formation of the triangular faces, the same 0.25 mL of $NH_2OH \cdot HCl$ was added, but (b3) 0.5 and (b4) 0.75 mL of 1 M NaOH need to be used. (c1−c4) Pentagonal prisms were converted to form star columns by increasing the volume of $NH_2OH \cdot HCl$ added (i.e., 0.15, 0.25, 0.45, and 0.65 mL).

but highly symmetrical nanocrystal structure has not been reported before. By increasing the volume of 0.2 M $NH_2OH \cdot HCl$ used to 0.25 mL, truncated stellated icosahedra were produced as described above. Further suppression of the triangular faces cannot be achieved by increasing the volume of $NH_2OH \cdot HCl$ added, as unusual particle morphologies derived from the interpenetrated growth of truncated octahedra and octahedra were formed (see Supporting Information, Figure S5). Instead, we found that by increasing the volume of 1 M NaOH added from 0.25 mL to 0.5 and 0.75 mL and keeping the volume of $NH_2OH \cdot HCl$ used at 0.25 mL, the height of protruded triangular faces of the truncated stellated icosahedra can be further reduced. From observation of the Cu_2O shell morphologies obtained by increasing the volume of $NH_2OH \cdot HCl$ added, it is presumed that the stellated icosahedra are formed as a result of the interpenetrated growth of truncated cubes. The highly faceted gold nanocrystals promote this unusual type of crystal growth. The interpenetrated growth mechanism for formation of the stellated icosahedra can be considered as two to three truncated cubes, at different orientations to one another, trying to form simultaneously from the same highly faceted gold nanocrystal core, which provides multiple surfaces at different angles for shell growth. The result is the formation of a Cu_2O crystal shell with 20 vertices, rather than a truncated cube with eight vertices when an octahedral gold nanocrystal is used for shell growth. If the gold nanocrystal core has a less symmetrical shape, imperfect Cu_2O polyhedra can form. In this regard, the truncated stellated icosahedra (Figure 1c) can be considered to be generated via the interpenetrated growth of cuboctahedra. For the case of using pentatwinned gold nanorods to grow core−shell structures, pentagonal prisms can be converted to form star columns by increasing the volume of $NH_2OH \cdot HCl$ added. The star columns contain five side branches derived from further growth of the barlike structures described above and represent as another unusual nanostructure morphology synthesized. As for the use of micrometer-sized Au plates as cores, no significant changes to the morphology of the concave Au−Cu_2O plates were found by increasing the reductant volume (see Supporting Information, Figure S6). This happens presumably because of the very large sizes of the Au plates.

The unique structures of stellated icosahedra and star columns were studied in detail (see Figure 6). Close examination of a single stellated icosahedron reveals that the triangular pyramids are actually slightly truncated at the top. Lattice fringes parallel to the truncated face were found to be the (111) lattice planes of Cu_2O. The top {111} face makes an angle of ~54° to a side face of the pyramid (see Figure 6b). This angle analysis suggests that each triangular pyramid of the stellated icosahedron is bounded by three {100} side faces and a {111} top face (see Figure 6c). This facet assignment is consistent with the idea that the stellated icosahedra are synthesized via the interpenetrated growth of truncated cubes. And the formation of the truncated stellated icosahedra (Figure 1c) with increased {111} surfaces and decreased {100} surfaces is related to the morphological evolution of Cu_2O from truncated cubes to cuboctahedra. A TEM image of the side view of a star column is shown in Figure 6d. Selected-area electron diffraction (SAED) pattern and HR-TEM image taken over a side branch of the star column indicate that the end face of the branch is the {100} face (Figure 6e,f). Angle analysis from the TEM and HR-TEM images reveals the end faces of the star column as the {111} faces. An SEM image of the end view of a star column shows that the side face of the branch is at an angle of about 45° to the end face, so the side faces of the branch are the {110} faces (Figure 6g). A schematic drawing of a star column with the faces indicated is provided in Figure 6h.

It would be interesting to see how these novel Au−Cu_2O core−shell heterostructures were synthesized. Their growth process has been investigated by examining some intermediate products formed during the reaction. Figure 7 presents TEM

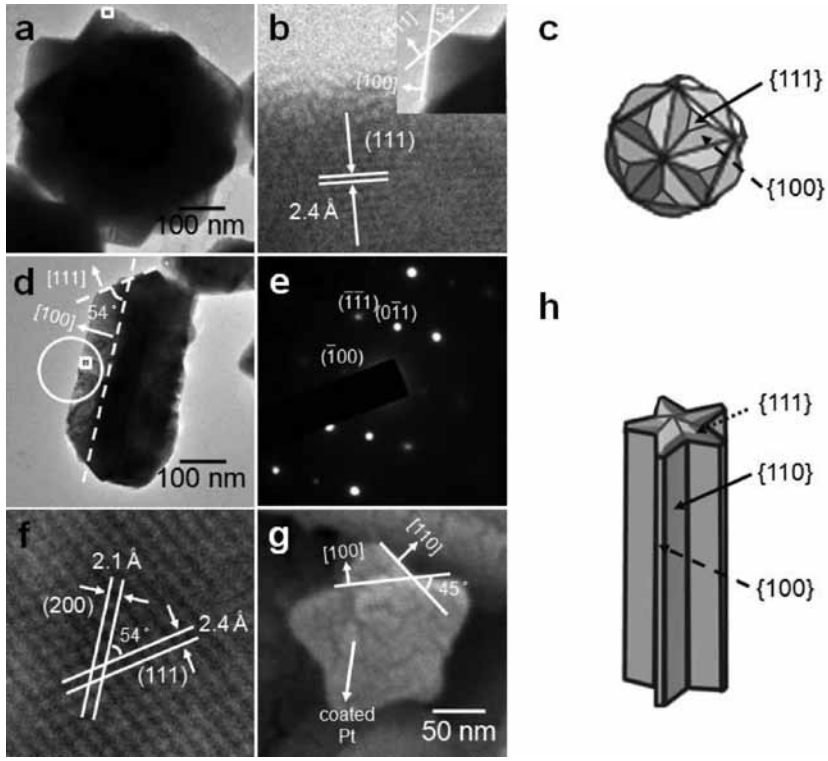

Figure 6. TEM characterization of a stellated icosahedron and a star column. (a) TEM image of a single stellated icosahedron. (b) HR-TEM image of the square region shown in panel a. The lattice fringes have a measured *d* spacing of 2.4 Å and should correspond to the (111) planes of Cu_2O. Angle analysis (~54° angle between the {111} face and the {100} face) reveals that each triangular pyramid is bounded by three {100} side faces and an {111} top face. (c) Drawing of a stellated icosahedron synthesized with the faces indicated. (d) TEM image of the side view of a star column. The end face is at an angle of 54° to the side face. (e) SAED pattern of a branch of the star column (circled region in panel d) taken along the [011] zone axis. (f) HR-TEM image of the square region in panel d, revealing the (200) planes of Cu_2O running parallel to the growth direction of the branch. The (111) planes run at an angle of 54° to the (200) planes. (g) SEM image of a star column viewed from an end. A Pt coating was applied to this sample for SEM imaging. Angle analysis suggests that each branch consists of an {100} end face and {110} side faces. (h) Drawing of a star column with the faces indicated.

images of the intermediate products collected after 1 (Figure 7a−d) and 10 (Figure 7e−j) min of reaction with the long gold nanorods as the cores. Many small Cu_2O particles with sizes of less than 10 nm have already been formed after reaction for just 1 min, as verified by the SAED patterns of the particles (Figure 7a−c). Some of these Cu_2O particles were found to adhere to the gold nanorods (Figure 7d). After 10 min of reaction, the Cu_2O shell has been partially formed through aggregation of the small particles (Figure 7e). Notice that the shell did not necessarily grow epitaxially over the surface of the nanorod as normally observed for the formation of core−shell structures; some regions of the shell can just grow around the rod without contacting the rod surface. This situation is reminiscent of the core−cage growth previously observed.[23] Figure 7f gives a TEM image of the end region of the nanorod revealing the epitaxial growth of the (111) planes of Cu_2O over the {111} end facets of the gold nanorod. Figure 7g shows another TEM image with the outer shell mostly formed around a gold nanorod. A close inspection revealed that small Cu_2O particles filled the space between the shell and the nanorod core (Figure 7h). This observation suggests that conformal epitaxial growth has not fully established over the entire surface of the nanorod even though the outer shell has been formed. Continued shell growth eventually lead to the formation of a crystalline shell structure (Figure 7i,j).

A similar growth mechanism was observed for the other Au−Cu_2O core−shell heterostructures. Figure 8 displays the TEM images of the intermediate products collected after 10 min of reaction leading to the formation of cuboctahedra, truncated stellated icosahedra, and concave plates. Remarkably, hollow Cu_2O shell structures at different growth stages can be observed around the gold cores. The overall framework structure clearly is constructed first before the space between the outer shell and the core is completely filled. Nevertheless, the shell is connected to the core via preformed Cu_2O bridges, through which the core can guide the growth of the shell with a proper orientation. This unusual hollow-shell-refilled (HSR) growth mechanism is different from the epitaxial overgrowth of shells on the surfaces of the core particles normally observed and has not been reported before. A schematic illustration of the HSR growth mechanism for the four different kinds of Au−Cu_2O heterostructures is available in Supporting Information, Figure S7. Hollow Cu_2O nanostructures with cubic, octahedral, and other shapes have been prepared by both templated and templateless synthesis methods, so the initial formation of hollow Cu_2O shells is possible.[29−33] Cu_2O nanocubes have also been observed to evolve from cubic nanocages.[34] Since the reaction conditions used here are similar to those in our previous study on the formation of Cu_2O nanocages but without the addition of HCl,

(29) Teo, J. J.; Chang, Y.; Zeng, H. C. *Langmuir* **2006**, *22*, 7369–7377.
(30) Wang, Z.; Wang, H.; Wang, L.; Pan, L. *J. Phys. Chem. Solids* **2009**, *70*, 719–722.
(31) Xu, Y.; Jiao, X.; Chen, D. *J. Phys. Chem. C* **2008**, *112*, 16769–16773.
(32) Lu, C.; Qi, L.; Yang, J.; Wang, X.; Zhang, D.; Xie, J.; Ma, J. *Adv. Mater.* **2005**, *17*, 2562–2567.
(33) Gao, J.; Li, Q.; Zhao, H.; Li, L.; Liu, C.; Gong, Q.; Qi, L. *Chem. Mater.* **2008**, *20*, 6263–6269.
(34) Yang, Z.; Chiang, C.-K.; Chang, H.-T. *Nanotechnology* **2008**, *19*, 025604.

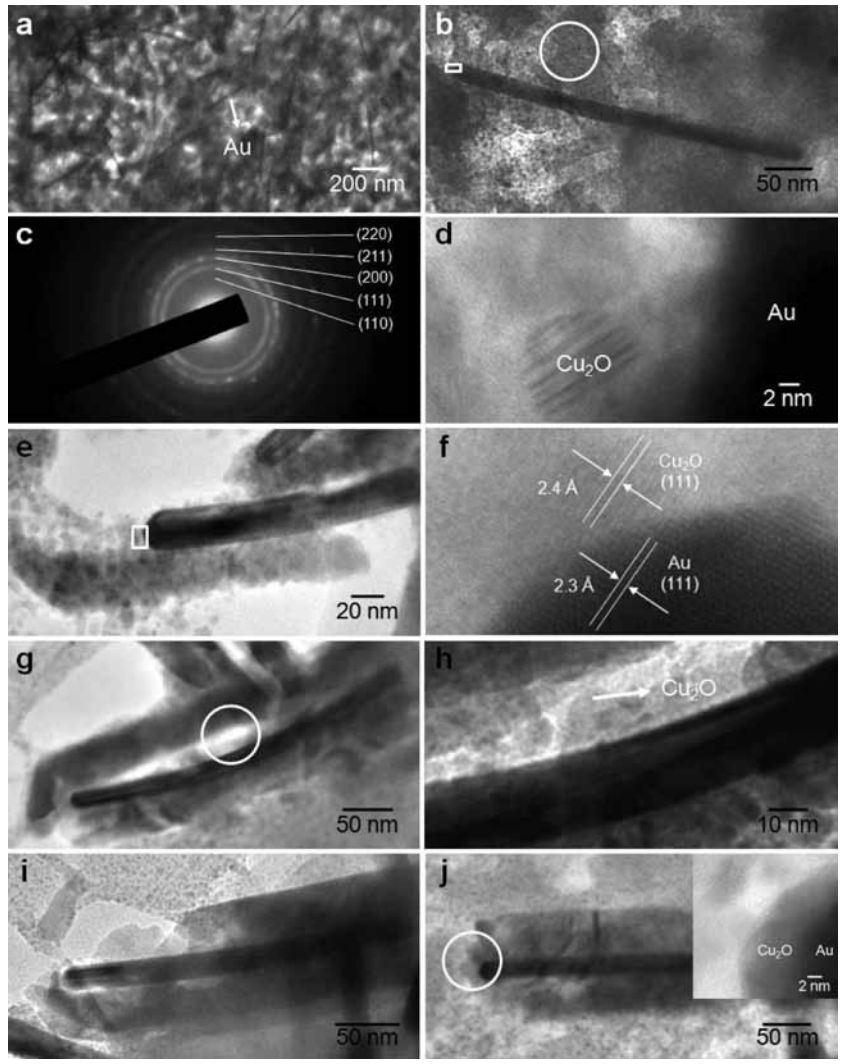

Figure 7. (a) TEM image of the product collected from the solution with 0.25 mL of $NH_2OH \cdot HCl$ added and after reaction for just 1 min. (b) TEM image of a single gold nanorod taken from this 1-min sample. Numerous small particles surrounding this nanorod were confirmed to be Cu_2O nanoparticles, as verified by the SAED pattern shown in panel c, taken over the circled region in panel b. (d) TEM image showing the rectangular region in panel b. A Cu_2O particle can be seen adhering to the Au surface. (e−j) TEM images of the intermediate products observed after 10 min of reaction. (e, g) Aggregation of the nanoparticles over the side surface of the nanorods and elongated growth of Cu_2O shells can be seen. The shells have not completely enclosed the nanorod cores. (f) HR-TEM image of the rectangular region in panel e, showing the epitaxial growth of Cu_2O. (h) TEM image of the circled region in panel g, showing tiny Cu_2O nanoparticles bridging the outer shell and the Au nanorod core. (i, j) With the overall shell structure established, continued growth eventually forms a closed shell. The images suggest that further growth tend to be confined to the ends of the nanorod heterostructures. Inset of panel j reveals the circled region.

it is not surprising that nanocages are formed first, enclosing the Au nanocrystal cores.[23] In a basic reaction condition, acidic etching is minimized. Continued shell growth leads to the eventual formation of the core−shell heterostructures. The tendency of Cu_2O to form cubic to octahedral structures under the current reaction conditions used,[20] and the epitaxial growth relationship with the gold cores defining the shell growth orientation and facets, result in the preparation of these unusual heterostructures.

Conclusion

In conclusion, we have synthesized unusual Au−Cu_2O core−shell heterostructures by use of Au nanoplates, nanorods, octahedra, and highly faceted nanoparticles as structure-directing cores for the overgrowth of Cu_2O crystals. Despite significant lattice mismatches between the different gold surfaces and the lattice planes of Cu_2O, these metal−semiconductor core−shell structures can still be prepared. These heterostructures are distinctly different from ordinary core−shell nanoparticles in that the cores exert a great influence on the morphology and orientation of the shells. Systematic morphological evolution of the shell structures can also be easily achieved. This synthetic approach also allows the formation of Cu_2O truncated stellated icosahedra and star columns that are rarely observed. The heterostructures have been found to be synthesized by an unusual HSR growth mechanism. Because some of these heterostructures possess complex structures with many exposed facets and edges, they may exhibit enhanced photocatalytic activity and catalytic properties. We have previously shown that Cu_2O octahedra and hexapods with many {111} facets are photocatalytically active, but sharp-faced Cu_2O cubes with only {100} facets are photocatalytically inactive.[22] The electronic properties of Cu_2O may be modified by the inclusion of gold cores. Our preliminary results on the electrical conductivity measurements of single Cu_2O and Au−Cu_2O core−shell cubes showed significantly better conductivity for the Au−Cu_2O cubes.

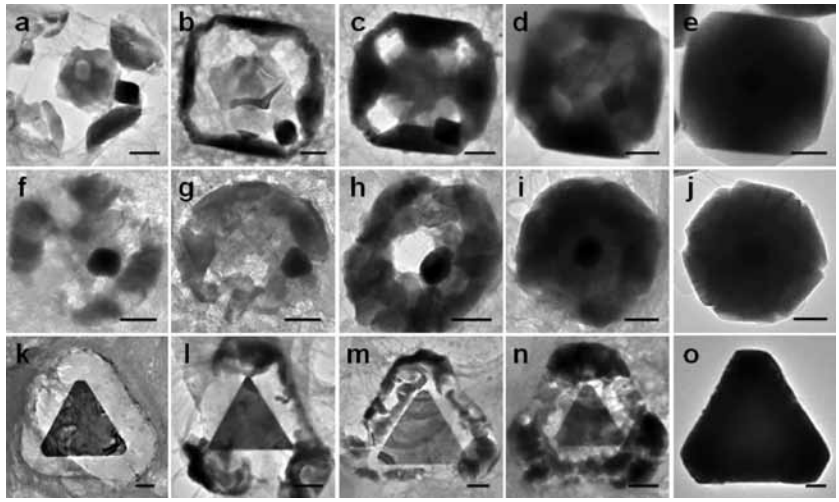

Figure 8. Observation of intermediate products formed for elucidation of the growth mechanism of these core−shell heterostructures. The intermediate products leading to the formation of (a−e) cuboctahedra, (f−j) truncated stellated icosahedra, and (k−o) concave plate structures were collected after 10 min of reaction. The TEM images are presented to show the possible sequence of shell formation. The last images show the final products. These images clearly reveal a hollow-shell-refilled (HSR) mechanism in which the overall shell structure is established first before the space between the shell and the core, connected by preformed Cu_2O bridges, is completely filled. The cores appear to move to one side of the shell, possibly due to the drying effect in the preparation of TEM samples. Scale bars for the first two rows are equal to 100 and 200 nm for the third row.

Other metal−Cu_2O core−shell heterostructures may also be synthesized by an approach similar to that described here. These are some of the interesting research directions that can be conceived with the use of these heterostructures.

Acknowledgment. This work was supported by the National Science Council of Taiwan (Grant NSC95-2113-M-007-031-MY3). We thank Hsin-Lun Wu for assistance in the synthesis of the highly faceted gold nanocrystal seeds. We also thank Dr. Chih-Chieh Wang for help in HR-TEM characterization of some samples and Lian-Ming Lyu for preparing samples for microtomy.

Supporting Information Available: Synthetic procedures for the various gold nanocrystal cores and their SEM images; TEM, HAADF-STEM, and EDS characterization of the core−shell heterostructures; SEM images of products formed from the highly faceted gold nanocrystal and plate cores with the addition of different amounts of $NH_2OH \cdot HCl$; and schematic illustration of the HSR mechanism. This material is available free of charge via the Internet at http://pubs.acs.org.

JA9065333